Article | Received 16 September 2025; Revised 19 October 2025; Accepted 25 October 2025; Published 7 November 2025
https://doi.org/10.55092/am20250010

# Process monitoring of P-GMAW-based wire arc direct energy deposition of stainless steels via time-frequency domain analysis and Isolation Forest

**Giulio Mattera[1,*], Elena Manoli[1], Zengxi Pan[2] and Luigi Nele[1]**

[1] Department of Chemical, Materials and Production Engineering, University of Naples Federico II, Naples, Italy
[2] School of Mechanical, Materials, Mechatronic and Biomedical Engineering, University of Wollongong, Wollongong (NSW), Australia

* Correspondence author; E-mail: giulio.mattera@unina.it.

## Highlights:

- Online identification of anomalies.
- Global and local Time-frequency features extraction.
- Comparison between Statistical Process Monitoring and Isolation Forest-based monitoring.
- One-class-based anomaly detection.

**Abstract:** Wire Arc Directed Energy Deposition (WA-DED) is emerging as a cost-effective method for fabricating large metallic components. Despite its robustness and high deposition rates, the process remains prone to instabilities and defects, making reliable monitoring essential for industrial adoption. However, most advanced monitoring strategies rely on large, labelled datasets, whose generation is costly and impractical in real manufacturing environments. This work proposes an unsupervised monitoring framework that learns normal behaviour exclusively from defect-free depositions and detects online deviations using welding current and voltage signals. A set of time–frequency features, comprising Fast Fourier Transform (FFT) descriptors and multi-level Discrete Wavelet Transform (DWT) statistics, was extracted to represent the signals. An Isolation Forest model was trained on in-control data and benchmarked against Statistical Process Monitoring (SPM) based on Shewhart control charts applied to time- and frequency-domain energy features. Validation on two multi-layer wall specimens containing both good and anomalous regions showed that the proposed approach achieved an F1-score of 85.3%, a 57% improvement over the best control chart (54.3%). The method exhibited greater sensitivity to arc-related instabilities while maintaining high precision and avoiding excessive false alarms. The framework requires no defect labels and only normal data for training, aligning with industrial constraints where labelled anomaly datasets are scarce. Limitations remain, notably the absence of defect localisation and the qualitative nature of alerts. Future work will address these aspects through the development of a quantitative quality index, improved localisation, and extension to complex geometries such as overhanging structures, alongside multi-sensor and multimodal fusion.

**Keywords:** WA-DED; process monitoring; machine learning; Isolation Forest; direct energy deposition

## 1. Introduction

Wire Arc Direct Energy Deposition (WA-DED), illustrated in Figure 1, is a Metal Additive Manufacturing (MAM) process in which arc welding technology is employed to fabricate large components through a layer-by-layer approach [1]. Various arc welding methods can be adopted for this process [2], including Tungsten Inert Gas [3], Plasma Arc Welding [4], and Metal Inert Gas (MIG)N [5], with MIG most commonly used due to its relative simplicity and the easier management of robotic tool paths [6,7].

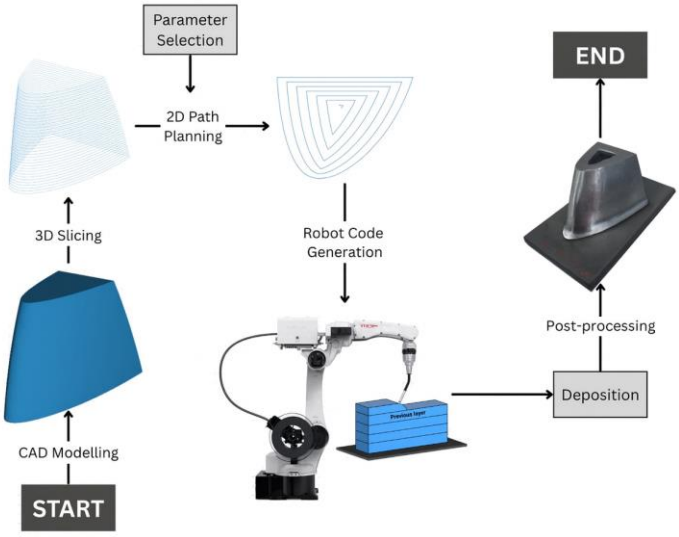


**Figure 1.** WA-DED process workflow.

Although several advancements have been introduced to improve the stability of short-circuit-based deposition—such as pulsed welding and controlled short-circuit systems [8], which enable deposition with reduced heat input and are suitable for various alloys—defects may still occur during the build. As shown in Figure 2, the most common defects are porosity and arc instabilities (e.g., spatter or inadequate shielding gas). These typically arise from incorrect feedback control during the process [9]. Less frequent defects include cracks and lack of fusion, which are often associated with improper management of heat input, potentially linked to factors such as poor adjustment of the arc length during deposition [10]. In addition, rarer issues such as humping, balling, or burn-through can occur due to the inappropriate selection of process parameters [11]. Process monitoring, therefore, plays a critical role in WA-DED, as it enables the detection of anomalies, the early termination of faulty builds, and the potential provision of corrective recommendations to the operator, thereby supporting more informed decision-making [12]. With respect to process monitoring, three main objectives can be identified. The first is state measurement, in which the geometry of each deposited layer is measured or estimated through models. The second is anomaly detection, which concerns identifying any deviations from normal behaviour. The third is classification, where each detected anomaly is assigned a specific meaning.

In state measurement, the key parameters are layer height, layer width, and arc length. Traditionally, these require the combined use of cameras for accurate measurement [13–15], but increasing efforts are now directed towards contactless sensing solutions [16,17].

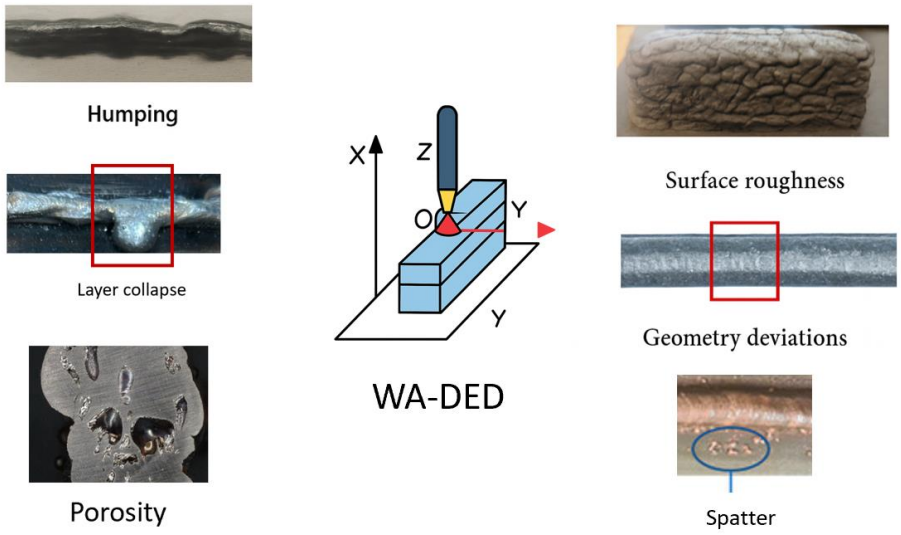


**Figure 2.** Typical defects of WA-DED process.

For anomaly detection, a range of signals may be employed, including camera-based monitoring [18,19], welding signals (arc current and voltage) [20,21], and acoustic emission [22]. Regarding vision-based monitoring systems, they have been employed to analyse weld pool geometry [23,24], droplet transfer dynamics [25], and surface irregularities [26], enabling real-time identification of defects and instabilities. In particular, two main approaches can be identified: the first directly processes the images acquired from welding cameras using Convolutional Neural Networks (CNNs) to assign a class to each frame, while the second employs more complex architectures, such as YOLO, to localise surface defects in real time. In both cases, machine learning is largely employed, since images are complex to process via traditional approaches. However, in industrial practice, welding signals are by far the most widely used, since they are cost-effective, non-intrusive, and align with established standards [27].

Conventional monitoring systems are derived from arc welding technology and typically rely on control charts applied to current or voltage signals [28,29]. More recent approaches have explored the use of supervised learning techniques, such as binary classifiers [30–32]. Although these methods have demonstrated promising results, their industrial adoption is hindered by the demanding requirement of generating large, labelled datasets. This process involves extensive experimental trials, destructive testing, and subsequent labelling, which is often impractical in real production environments. Consequently, despite advances in machine learning, the industry still largely relies on control chart methods, as these require only normal process data to operate effectively. Nevertheless, control charts are often unable to capture subtle or rapid anomalies. For this reason, new approaches have been developed based on the unsupervised learning paradigm. Unsupervised learning, as an alternative, eliminates this complex data labelling and can detect anomalies by identifying patterns deviating from the expected behaviour, using solely normal data for training [33,34] thus simplifying the task in an operational industrial setting. While time domain signals offer a degree of information, frequency domain analysis

emerges as a valuable tool for extracting a diverse range of information across different frequency bands, particularly crucial due to the close connection between welding waveform frequency content and droplet frequency [35]. The latter, representing the rate of molten metal droplet transfer, is essential for monitoring and controlling welding processes to prevent defects in weld bead geometry and microstructure. Although several studies have employed frequency- or time–frequency-domain analysis for welding process monitoring, few have combined wavelet-based feature extraction with unsupervised anomaly detection. This work introduces a hybrid framework that integrates Discrete Wavelet Transform (DWT) features with the Isolation Forest algorithm to identify process anomalies without labelled data. The proposed method is also benchmarked against conventional Statistical Process Monitoring (SPM) techniques, enabling a direct comparison between frequency-based feature analysis and traditional mean-value approaches. Finally, the impact of time–frequency analysis is critically discussed in relation to SPM methods, highlighting the inherent limitations of conventional monitoring techniques. Based on previous studies that have highlighted the importance of frequency analysis and feature extraction for monitoring applications across different materials and processes, this work presents an approach in which an unsupervised learning-based monitoring framework is developed once features have been extracted from the time–frequency domain. In particular, data were collected during a P-GMAW process of 316L stainless steel, and the proposed monitoring method is applied to data associated with the production of a component.

## 2. Materials and methods

### *2.1. Experimental data collection*

The experimental system used to collect the data for this study consists of a Yaskawa AM2010 robotic station integrated with a Lincoln PowerWave 500 welding machine. The welding signals—current and voltage—were acquired using a National Instruments 6003 device, with a dedicated Python script developed with the nidaqmx library to record the signals at a sampling frequency of 5 kHz. The material employed was a 316L stainless steel wire with a diameter of 1.2 mm, deposited using the Pulsed Gas Metal Arc Welding (P-GMAW) process through the synergic line developed by Lincoln. A total of 72 parameter combinations, reported in Table 1, were used to collect data, with Contact Tip to Workpiece Distance (CTWD) with a shielding gas mixture of 80% Ar and 20% $CO_2$, and parameters fixed at a nozzle-to-work distance of 15 mm and a gas flow rate of 22 L/min, respectively.

The quality of the deposited layers was assessed by visual inspection and by analysis of the acquired welding signals. Given that the welding speed and the specimen length were known, the first and last seconds of each deposition were excluded from the analysis. Labels were then assigned to each one-second window of the recorded signals, which is a standard reference length for process monitoring in WA-DED. These labels were associated with the corresponding portion of the deposited layer. Figure 3 shows the experimental setup, an example of the recorded waveforms, and representative deposited layers exhibiting typical defects.

**Table 1.** Design of experiment conducted in this study.

| N | UltimArc | Welding speed [mm/min] | Wire feed speed [m/min] | Welding voltage [V] | Anomaly |
|---|---|---|---|---|---|
| 1 | −8 | 552 | 6.5 | 23 | 0 |
| 2 | −6 | 552 | 6.5 | 23 | 0 |
| 3 | −4 | 552 | 6.5 | 23 | 0 |
| 4 | −2 | 552 | 6.5 | 23 | 0 |
| 5 | 2 | 552 | 6.5 | 23 | 0 |
| 6 | 4 | 552 | 6.5 | 23 | 0 |
| 7 | 6 | 552 | 6.5 | 23 | 0 |
| 8 | 8 | 552 | 6.5 | 23 | 0 |
| 9 | 0 | 552 | 6.5 | 18 | 1 |
| 10 | 0 | 552 | 6.5 | 20 | 1 |
| 11 | 0 | 552 | 6.5 | 28 | 0 |
| 12 | 4 | 552 | 6.5 | 28 | 0 |
| 13 | 4 | 552 | 6.5 | 20 | 0 |
| 14 | 4 | 552 | 6.5 | 18 | 1 |
| 15 | −4 | 552 | 6.5 | 18 | 1 |
| 16 | −4 | 552 | 6.5 | 28 | 0 |
| 17 | −4 | 552 | 6.5 | 20 | 0 |
| 18 | 8 | 552 | 6.5 | 20 | 0 |
| 19 | 8 | 552 | 6.5 | 28 | 0 |
| 20 | 8 | 552 | 6.5 | 18 | 1 |
| 21 | −8 | 552 | 6.5 | 18 | 1 |
| 22 | −8 | 552 | 6.5 | 28 | 0 |
| 23 | −8 | 552 | 6.5 | 20 | 0 |
| 24 | 2 | 552 | 6.5 | 20 | 0 |
| 25 | 2 | 552 | 6.5 | 28 | 0 |
| 26 | 2 | 552 | 6.5 | 18 | 1 |
| 27 | −2 | 552 | 6.5 | 18 | 1 |
| 28 | −2 | 552 | 6.5 | 28 | 0 |
| 29 | −2 | 552 | 6.5 | 20 | 0 |
| 30 | 0 | 552 | 4.5 | 23 | 0 |
| 31 | 4 | 552 | 4.5 | 23 | 0 |
| 32 | −4 | 552 | 4.5 | 20 | 0 |
| 33 | −4 | 552 | 4.5 | 23 | 0 |
| 34 | 4 | 552 | 4.5 | 20 | 0 |
| 35 | 0 | 552 | 4.5 | 20 | 0 |
| 36 | 0 | 552 | 4.5 | 18 | 0 |
| 37 | −4 | 552 | 4.5 | 18 | 0 |
| 38 | 4 | 552 | 4.5 | 18 | 0 |
| 39 | 0 | 552 | 4.5 | 23 | 0 |

**Table 1.** *Cont.*

| N | UltimArc | Welding speed [mm/min] | Wire feed speed [m/min] | Welding voltage [V] | Anomaly |
|---|---|---|---|---|---|
| 40 | 4 | 552 | 4.5 | 23 | 0 |
| 41 | 4 | 552 | 4.5 | 20 | 0 |
| 42 | 0 | 552 | 4.5 | 20 | 0 |
| 43 | 0 | 552 | 4.5 | 18 | 0 |
| 44 | 4 | 552 | 4.5 | 18 | 0 |
| 45 | 4 | 750 | 6.5 | 25.2 | 0 |
| 46 | 4 | 750 | 4.5 | 21 | 0 |
| 47 | −4 | 750 | 6.5 | 25.2 | 0 |
| 48 | −4 | 750 | 4.5 | 21 | 0 |
| 49 | 8 | 750 | 4.5 | 21 | 0 |
| 50 | 8 | 750 | 6.5 | 25.2 | 0 |
| 51 | −8 | 750 | 6.5 | 25.2 | 0 |
| 52 | −8 | 750 | 4.5 | 21 | 0 |
| 53 | 0 | 750 | 3 | 16 | 0 |
| 54 | 10 | 750 | 3 | 16 | 0 |
| 55 | −10 | 750 | 3 | 16 | 0 |
| 56 | 0 | 750 | 2 | 14.7 | 1 |
| 57 | 10 | 750 | 2 | 14.7 | 1 |
| 58 | −10 | 750 | 2 | 14.7 | 1 |
| 59 | −10 | 550 | 2 | 14.7 | 1 |
| 60 | 0 | 550 | 2 | 14.7 | 1 |
| 61 | 10 | 550 | 2 | 14.7 | 1 |
| 62 | 10 | 550 | 3 | 16 | 0 |
| 63 | −10 | 550 | 3 | 16 | 0 |
| 64 | 0 | 550 | 2 | 16 | 1 |
| 65 | 0 | 750 | 2 | 16 | 1 |
| 66 | −10 | 550 | 2 | 16 | 1 |
| 67 | 10 | 550 | 2 | 16 | 1 |
| 68 | 4 | 750 | 2 | 16 | 1 |
| 69 | −4 | 750 | 2 | 16 | 1 |
| 70 | −10 | 750 | 2 | 16 | 1 |
| 71 | 10 | 750 | 2 | 16 | 1 |
| 72 | 4 | 550 | 2 | 16 | 1 |

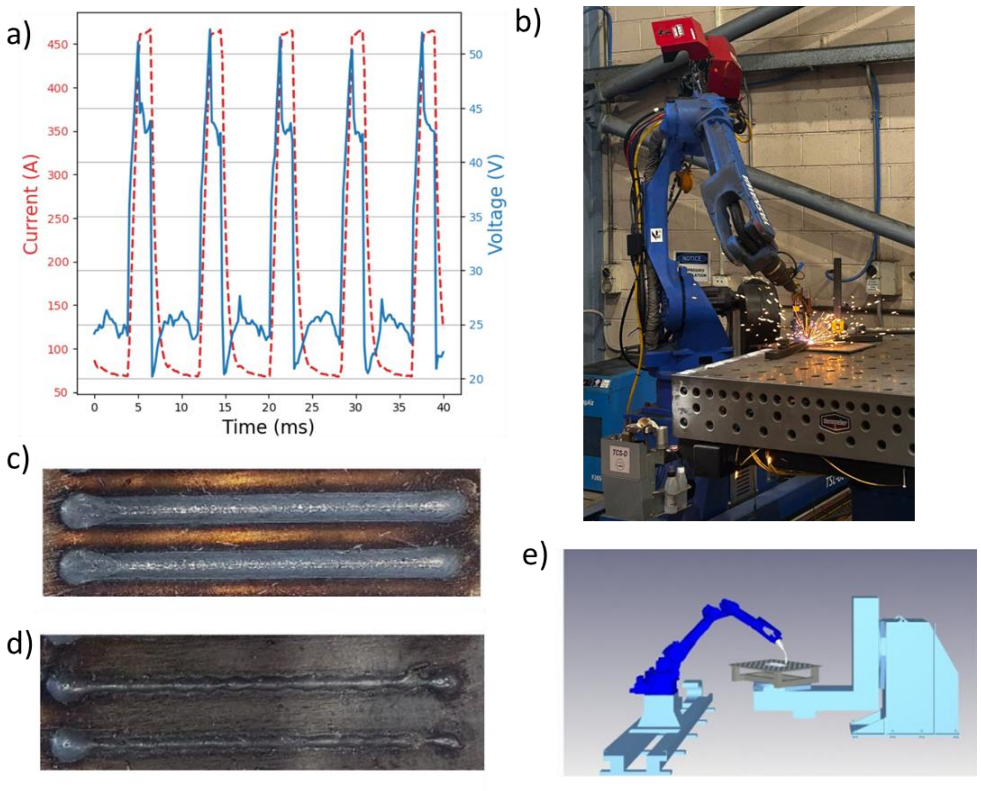


**Figure 3.** Summary of experimental procedure: **(a)** example of collected P-GMAW welding current and voltage data; **(b)** Real system employed planning; **(c)** good quality deposited layers; **(d)** poor quality and; **(e)** Digital model used for programming.

The 72 combinations of process parameters were obtained by varying the welding speed in the range of 552 to 750 mm/min, which resulted in thinner layers being deposited at higher speeds. The wire feed speed (WFS) was adjusted between 2 and 6.5 m/min, while the reference welding voltage ranged from 14.7 to 23 V, both contributing to the deposition of thicker layers as their values increased. Another parameter that was varied was the UltimArc$^{TM}$ setting, which enhances deposition rate and arc stability by adjusting the pulse frequency (see Figure 4). This parameter was varied between –8 and +8.


**Figure 4**. Effect of UltimArc$^{TM}$ parameter on frequency waveform in P-GMAW process.

Once the data had been collected, it was segmented into windows of one second to match the granularity of the assigned labels. To evaluate the performance of the monitoring algorithm, the dataset was then divided into training and testing sets. Specifically, 80% of the data corresponding exclusively to defect-free layers (anomaly = 0) was used for training, while the remaining data—including both

sound and defective depositions—was reserved for testing. Finally, to demonstrate the effectiveness of the proposed monitoring methodology in assessing the quality of real multi-bead, multi-layer components, a WA-DED part was fabricated (Figure 5) by employing the digital model shown in Figure 3b to program the robot. The developed method was applied to this component, and the obtained results were analysed and compared.

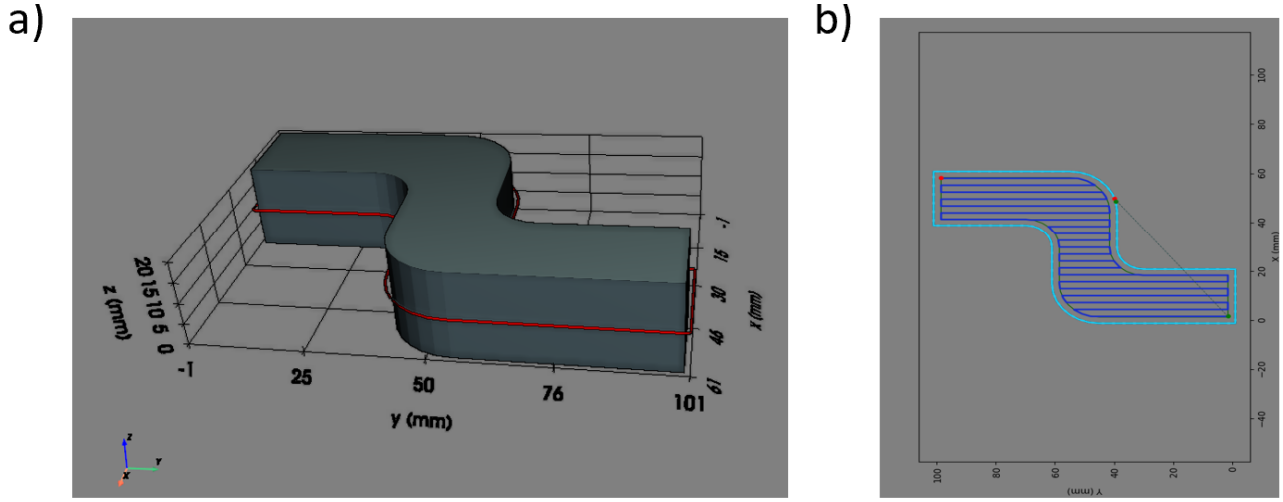


**Figure 5. (a)** CAD model of the part to be produced; **(b)** example of the path planning strategy, distinguishing between the external contour and the infill.

*2.2. Statistical process monitoring*

In this work, the aim is to compare the proposed time–frequency feature extraction combined with clustering against traditional monitoring methods. As a baseline, a Shewhart control chart is employed [36]. The underlying principle of the control chart, shown in Figure 6, is to use defect-free data, defined as in-control since the process operates within the bounds where no defects occur. An anomaly is detected when the input data exceeds the threshold defined by the mean $(\mu) \pm 3$ standard deviations $(\sigma)$.

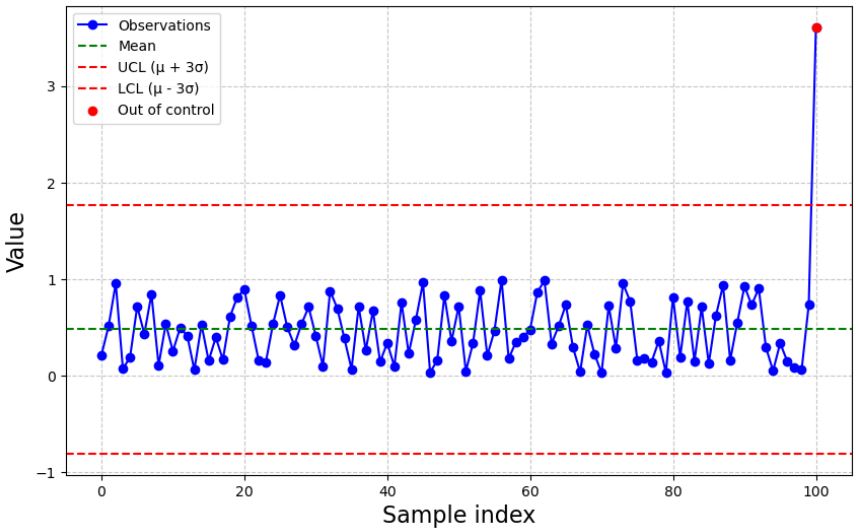


**Figure 6.** Example of a Shewhart control chart. Control limits are estimated from in-control training data; samples exceeding $\mu \pm \sigma$ are flagged as out of control.

Although the control chart can be applied to any signal, its main limitation is that, by construction, it is univariate, meaning it can only monitor one variable at a time [37]. The standard approach typically involves tracking either the welding current or voltage [38]. However, monitoring single raw samples at the acquisition rate is not meaningful; therefore, aggregated metrics—such as the mean or the signal energy—are usually employed. In this work, we implemented control charts for:

- the energy of the welding current,
- the energy of the welding voltage,
- the energy of the power spectral density (PSD) of the welding current, and
- the energy of the PSD of the welding voltage.

The Power Spectral Density (PSD) describes how the power of a signal is distributed across frequencies, providing insight into its dominant components. Previous studies have shown that defects or anomalies in WA-DED alter the spectral signature: arc instabilities typically increase energy at higher frequencies, spatter, porosity, and short circuits appear as localised spikes or spectral shifts, while stable deposition concentrates energy within expected frequency bands (e.g. the pulse frequency). Therefore, monitoring the total PSD energy, or the energy within specific bands, thus offers a compact indicator of process stability. In this work, the PSD was computed using Welch's method. Briefly, the Welch method divides the signal into k segments of length N, with an overlap of D (N = 1024 and D = 64 in this work). Each segment is multiplied by a Hamming window ( $w_0[n] = 0.54 + 0.46\cos\left(2\pi n/N-1\right)$ ) to reduce spectral leakage, and the periodogram is then computed as shown in Equation (1), where U is a normalisation factor that preserve the power and depends by the hamming window.

$$P_k(f) = \frac{1}{U \cdot N}\left|\sum_{n=0}^{N} x_k[n] \cdot w_o[n] e^{-j2\pi fn}\right|^2 \quad (1)$$

The resulting PSD is a frequency-domain vector, whose integration over all frequency bins (summation in the discrete case $\sum P_k$) yields the corresponding energy of the PSD. This sum reduces the variance of the PSD estimate compared to a single periodogram, at the cost of reduced frequency resolution. However, this approach allows for a comparison between traditional and proposed monitoring techniques, while also highlighting the potential advantages of using time–frequency features over conventional time-domain metrics in control chart applications.

### *2.3. Time-frequency features extraction*

As discussed, frequency-domain analysis plays a crucial role in data processing and machine learning, particularly for extracting meaningful features from time series signals. Two widely employed techniques for this purpose are the Fast Fourier Transform (FFT) and wavelet analysis. The FFT transforms a waveform from the time domain to the frequency domain, representing the signal in terms of its constituent sinusoidal components. In contrast, wavelet analysis is a time–frequency method that offers greater flexibility than the FFT. Specifically, the wavelet transform can analyse signals with complex frequency content using different basis functions, such as Gaussian or Morlet wavelets, thereby enabling analysis across multiple scales. Furthermore, unlike the FFT, the wavelet transform preserves temporal information, making it particularly suitable for non-stationary signals.

More in detail, the FFT reveals the amplitudes of the sinusoidal components at different frequencies that characterise the signals. Typically, before computing the FFT, the signal is centred around its mean

in order to remove the DC component. This step is important, as the DC offset is a dominant factor in the welding process and can obscure the subtler variations across other frequency bands. This procedure is valid for both welding current and welding voltage signals. Once the FFT has been obtained, statistical descriptors such as the energy, mean, standard deviation, variance, and kurtosis can be extracted to characterise the deposition quality (5 features per signal). In fact, when an anomaly occurs, the FFT spectrum often changes, leading to different amplitudes and shifts in the dominant frequencies. These variations alter the statistical descriptors, reflecting the modified distribution of spectral components. A total of 5 descriptors are extracted per signal, resulting in 10 features for the two-channel case (welding voltage and welding current). These descriptors, derived from the FFT analysis, capture the overall frequency-domain behaviour of the signals, since temporal information is inherently lost during the transformation. Together, they provide a richer basis for distinguishing between normal and anomalous welding behaviour. An example of the FFT over a 1-second deposition window is shown in Figure 7, where a stable transfer is compared with an unstable condition. The latter arises from a variation in CTWD, with a hump generated as a consequence of an undercut in the previously deposited layer, which is characterised by a noticeable increase in the response within the low-frequency bandwidth.

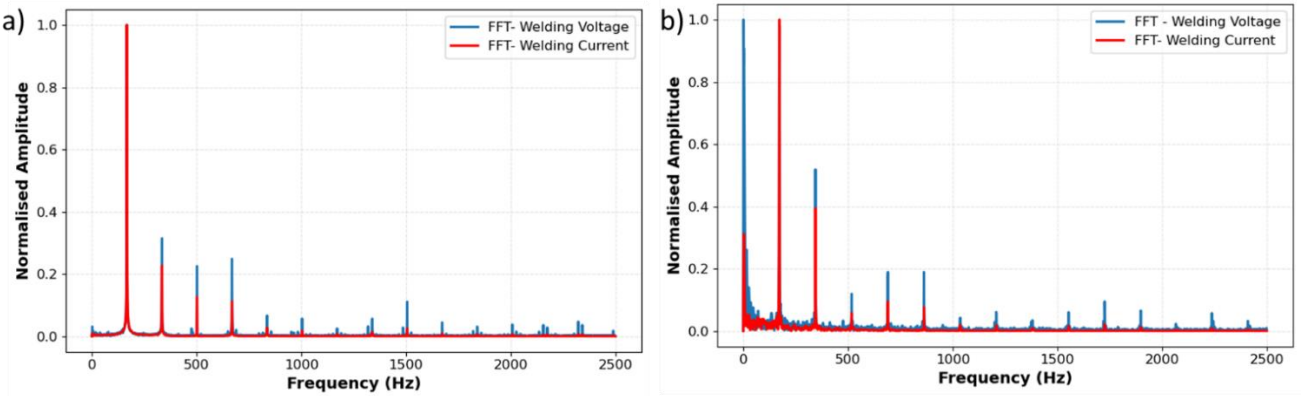


**Figure 7.** FFT of welding voltage and current signals during WAAM deposition. **(a)** Stable deposition, characterised by a dominant frequency component and regular harmonic peaks, indicating consistent droplet transfer and arc stability; **(b)** Deposition affected by a humping defect, showing additional frequency components and irregular amplitude distribution associated with arc and metal transfer instability.

However, because temporal information is lost, the FFT may struggle to localise defects, and rapid frequency changes associated with defect formation may not be immediately evident in the overall deposition. In such cases, more advanced methods, such as the wavelet transform, can be applied using the same underlying concept but with superior performance, as they adapt more effectively and extract richer information from signals whose frequency content varies over time. While the FFT remains useful for analysing the overall frequency distribution, it is less effective at capturing subtle variations, particularly those associated with defect onset. For signals with time-varying spectral characteristics, the Discrete Wavelet Transform (DWT) therefore provides a more suitable alternative.

As shown in Figure 8, the DWT is performed by applying a wavelet of predefined shape to the signal, which is then decomposed into several frequency bands represented by successive detail

coefficients. As in the case of FFT analysis, statistical descriptors can also be extracted at each level of decomposition, thereby increasing the amount of information available for process monitoring.

In this work, a five-level wavelet decomposition was performed using a fourth-order Daubechies wavelet, enabling the extraction of features across the following frequency bands: 2500–1250 Hz, 1250–625 Hz, 625–312.5 Hz, 312.5–156.2 Hz, 156.2–78.1 Hz, and 0–78.1 Hz. Since statistical descriptors were extracted at each level of the DWT, an additional 24 features were obtained per signal, resulting in a total of 56 features.

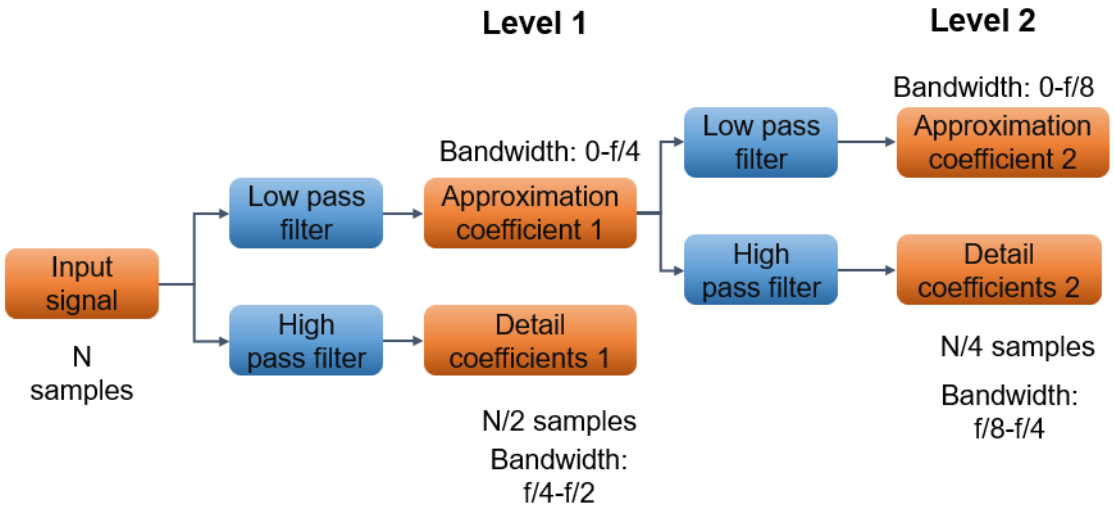


**Figure 8.** Example of decomposition levels in a DWT. The figure shows how the original signal is decomposed into approximation (low-frequency) and detail (high-frequency) components across multiple levels. Each level captures different frequency bands, enabling time–frequency localisation and effective analysis of non-stationary welding signals such as those in WAAM.

*2.4. Isolation Forest for online anomaly detection*

As discussed in the introduction, anomaly detection is a fundamental component of process monitoring systems. Its role is to identify abnormal states or irregular process conditions that, in manufacturing, may evolve into defects and consequently result in rejected parts. Reliable anomaly detection therefore contributes directly to process quality assurance and operational efficiency. In industrial practice, control charts represent one of the most established methods for anomaly detection, since their implementation rely only on few in control data. Indeed, their logic can be interpreted as a form of one-class learning. The procedure typically unfolds in two phases:

- Phase I (modelling): data representing only the "in-control" state are used to estimate control limits through simple statistical rules.
- Phase II (validation and testing): the derived limits are applied first to a validation subset of in-control data, and subsequently to new data that may include both in-control and out-of-control samples.

If the validation results are satisfactory—commonly with accuracies in the range of 90%–95%—the model proceeds to testing, where performance is assessed through standard metrics such as precision, recall, and F1-score, computed as in Equation 2–4. These measures quantify the proportion of false positives and undetected anomalies. In practice, the industrial relevance of these results depends on the application: if the

detection module merely generates an operator warning, false alarms may be tolerated. Conversely, if an alarm triggers a process interruption or part rejection, reducing false positives becomes critical.

$$p = \frac{TP}{TP + FP} \tag{2}$$

$$re = \frac{TP}{TP + FN} \tag{3}$$

$$Flscore = \frac{\left(1+\beta^2\right)\cdot p \cdot re}{\beta^2 \cdot p + re} = \frac{2p \cdot re}{p + re} \tag{4}$$

The Statistical process monitoring (SPM) approaches are generally univariate and therefore limited when handling complex, multidimensional data. Therefore, Machine learning methods provide a natural extension. In particular, one-class learning and semi-supervised approaches aim to learn directly the normality pattern of the data. Such methods allow the integration of richer feature sets, for example those obtained from time–frequency analysis, where secondary low- or high-frequency components emerge alongside the dominant frequency. These patterns, invisible to univariate monitoring, can reveal specific types of process anomalies. Machine learning algorithms can automatically learn the multidimensional representation of normal behaviour and subsequently classify new observations as either normal or anomalous.

Among the most effective machine learning algorithms for anomaly detection is the Isolation Forest [39]. The method builds upon the principle that anomalies are easier to isolate than normal points. A single decision tree randomly splits the feature space, and the number of splits required to isolate a point determines its anomaly score: the fewer the splits, the higher the likelihood of anomaly. While a single tree lacks robustness in high-dimensional settings, an Isolation Forest aggregates the results of multiple trees. Similar to Random Forest, it employs bootstrapping both across samples and features, ensuring variability and generalisation. Final anomaly scores are computed by averaging across trees or applying a majority voting scheme. In this study, the Isolation Forest was employed as the primary anomaly detection model. Hyperparameter selection, specifically the number of trees, was guided by validation performance. The optimal configuration was identified as that yielding validation accuracies in the range of 95%–97% on test data, ensuring both robustness and generalisability. The difference between SPM and Isolation Forest is illustrated in Figure 9.

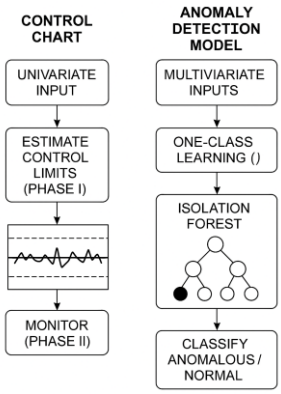


**Figure 9.** Difference between SPM-based and ML-based one-class monitoring.

## 3. Results

In this section, the results of the four SPM methods are discussed, followed by those obtained with the Isolation Forest methodology applied to time–frequency domain features. Subsequently, the performance of the best SPM model is compared with that of the proposed methodology, with reference to the reprinting of the component introduced in the *Materials and Methods* section. The methodologies are trained with a training dataset of 202 samples, exclusively composed of normal operating conditions, and tested on a test dataset of 551 samples that includes both normal and anomalous cases. Finally, a summary is provided, together with the main limitations and directions for future work. This concluding discussion highlights new research perspectives arising from the present study, in connection with the state of the art briefly outlined in the Introduction.

### *3.1. Process monitoring with control charts*

The proposed control chart methodology was applied to the test dataset using four different features: energy of the current signal, energy of the voltage signal, spectral energy of the current signal (via power spectral density, PSD), and spectral energy of the voltage signal. Additionally, an ensemble rule was implemented, in which a segment was classified as anomalous if any of the four individual charts indicated an out-of-control condition. Regarding the control chart based on the energy of the voltage signal (shown in Figure 10) achieved the precision of 100%, with a recall of 29% and an F1-score of 45%. The confusion matrix indicates that the method was able to correctly identify 43 anomalies, while misclassifying 105 anomalous cases as normal. This outcome highlights the limited effectiveness of time-domain current control charts in identifying anomalies, since they capture only a small fraction of the anomalous events. However, they also exhibit the advantage of not generating false alarms. This behaviour can be explained by the characteristics of the dataset, where the majority of anomalies are associated with variations in CTWD, inadequate shielding gas conditions, or unstable transfer modes. These phenomena primarily affect the voltage signal rather than the current, and may lead to energy values that resemble those of normal operating conditions in the time domain. Indeed, with the current control chart, no anomalies have been identified, as shown in Figure 11.

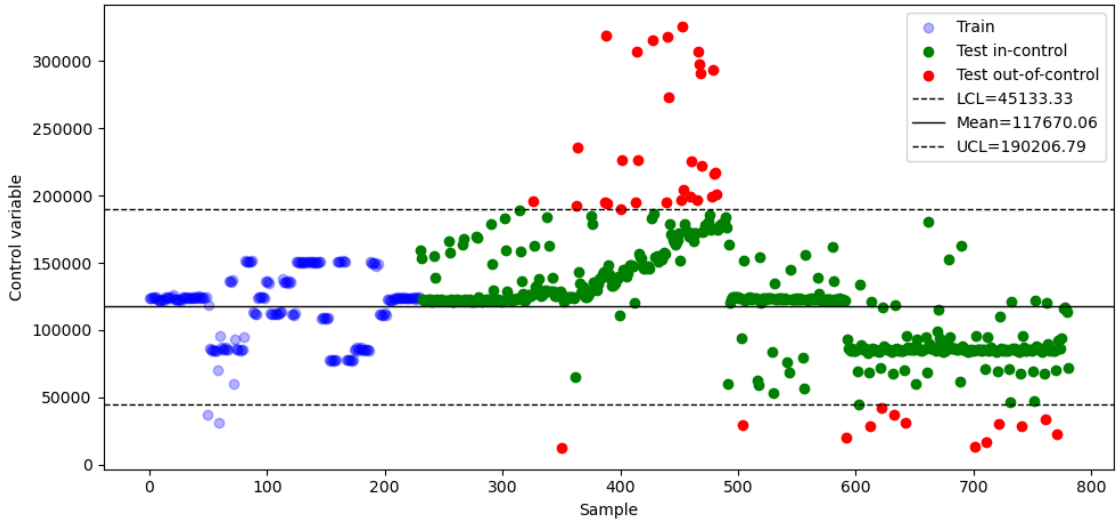


**Figure 10.** Control chart with mean and control bounds for the energy of the welding voltage.

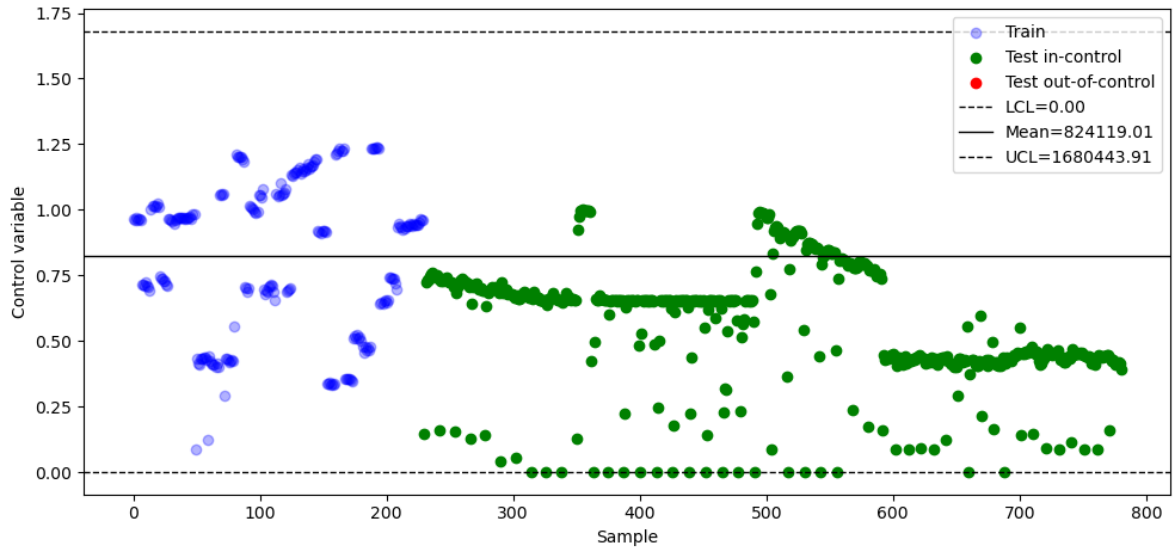


**Figure 11.** Control chart with mean and control bounds for the energy of the welding current.

Since frequency-domain information is assumed to play an important role, the PSD-based control chart of the current channel is reported in Figure 12. As expected, this feature enhanced the ability to detect anomalies, achieving a precision of 48.2%, recall of 62.2%, and an F1-score of 54.3%. Compared with the time-domain energy chart, the PSD representation increased the recall, correctly detecting 92 anomalies, also if at the cost of a higher number of false alarms (99). This result highlights the complementary nature of frequency-domain descriptors in anomaly detection. Similar behaviour was observed for the current signal (see Figure 13), although with a lower discriminative capability, leading to an F1-score of approximately 43.3%, enabling the detection of the anomalies rather the time domain.

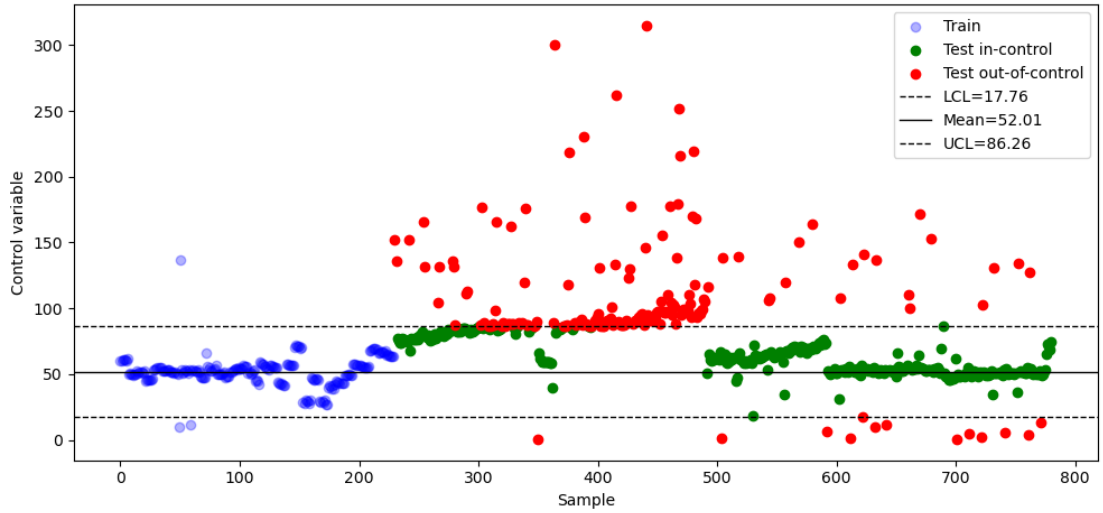


**Figure 12.** Control chart with mean and control bounds for the PSD energy of the welding voltage.

The quantitative results reported in Table 2 demonstrate that the models based on current-related features exhibit markedly lower detection performance compared to those derived from voltage. This outcome is consistent with the nature of waveform-controlled GMAW processes, in which the current is actively regulated to maintain a predefined waveform, whereas the voltage varies dynamically in response to arc conditions. As a result, voltage signals capture a higher degree of process variability and are more effective for detecting anomalies associated with instability in the metal transfer or arc behaviour.

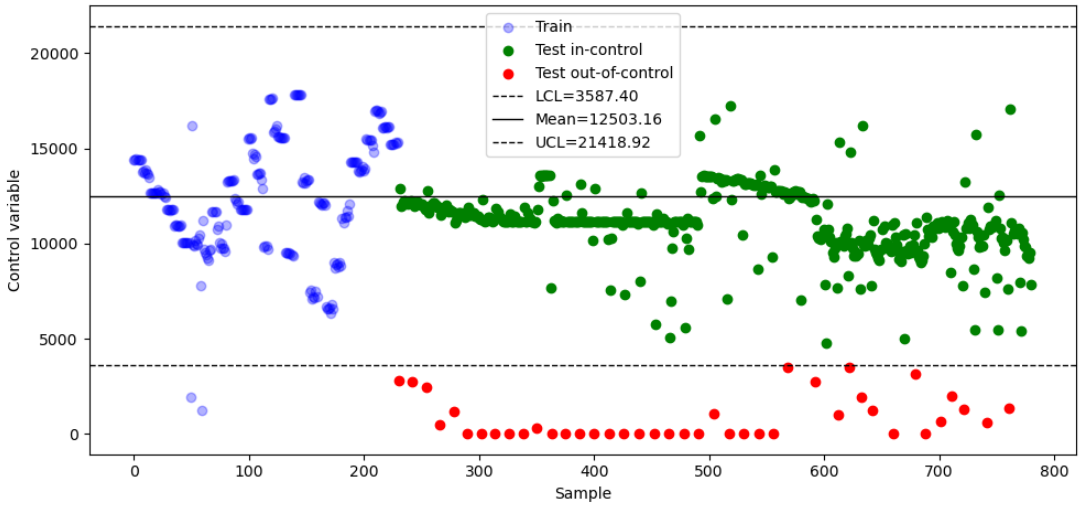


**Figure 13.** Control chart with mean and control bounds for the PSD energy of the welding current.

**Table 2.** Comparison of the obtained results (SPM *vs.* ML monitoring).

| Method | Precision | Recall | F1-score | Notes |
|---|---|---|---|---|
| SPM-Energy Voltage | **100%** | 29.5% | 45.0% | High precision, low sensitivity. With the current chart, no anomalies have been detected. |
| SPM-PSD Energy Voltage | 48.2% | 62.2% | 54.3% | Balanced but low performance |
| SPM-PSD Energy Current | 100% | 27.7% | 43.3% | No false alarms, low coverage |
| ML-Isolation Forest | 93.5% | **78.4%** | **85.3%** | No false alarms, strong performance |

### *3.2. Process monitoring with machine learning*

Following the methodology outlined in the previous chapter, a total of 56 features were extracted from the dataset. An Isolation Forest model comprising 300 trees and a contamination rate of 0.1 was trained on a random 70% subset of the feature matrix, while the remaining 30% was retained for validation. To determine the optimal hyperparameter configuration, several combinations of the number of trees (n_estimator) and contamination levels were systematically evaluated. Figure 14 illustrates the influence of the number of trees on model performance, whereas Figure 15 depicts the effect of varying contamination ratios. The highest overall performance in terms of F1-score (0.867) was achieved with 500 estimators and a contamination rate of 0.10, representing a robust balance between precision (0.959) and recall (0.791). Lower contamination values (0.05) yielded high precision but limited recall, indicating that many anomalies were not detected. Conversely, higher contamination levels (0.20) increased recall substantially but at the expense of precision, leading to a higher rate of false positives. Intermediate contamination values (0.10) consistently provided the most balanced results across all ensemble sizes.

The experiments confirmed that both parameter sets—(500, 0.10) and (300, 0.10)—deliver strong performance. In particular, the configuration with 500 trees maximises the overall F1-score, thanks to improved performance, whereas the configuration with 300 trees offers a more favourable trade-off, achieving a slightly higher recall. This makes the configuration with 300 estimators particularly suitable for applications in which comprehensive anomaly detection is prioritised over marginal gains in precision. The validation stage confirmed the robustness of the selected hyperparameters, with only five

being incorrectly classified as anomalies, corresponding to an accuracy of 92.7%. Once validated, the model was applied to the test set, yielding highly satisfactory results. Specifically, the model achieved a precision of 93.5%, corresponding to eight false alarms, and a recall of 78.4%, demonstrating strong anomaly detection capability. The resulting F1-score of 85.3% is consistent with, and in some cases superior to, values reported in the literature. Notably, this represents a 57% improvement in F1-score compared with the best-performing control chart. The confusion matrix further illustrates the classifier's effectiveness, showing that 116 anomalies were correctly identified, while 32 were missed. The complete set of results, including comparisons with control-chart-based methods, is summarised in Table 2.

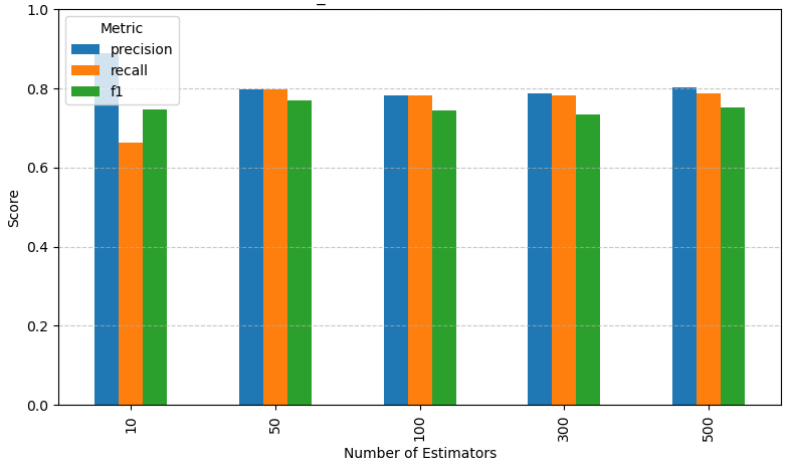


**Figure 14.** Effect of the number of trees on Isolation Forest performance, with contamination equal to 0.05.

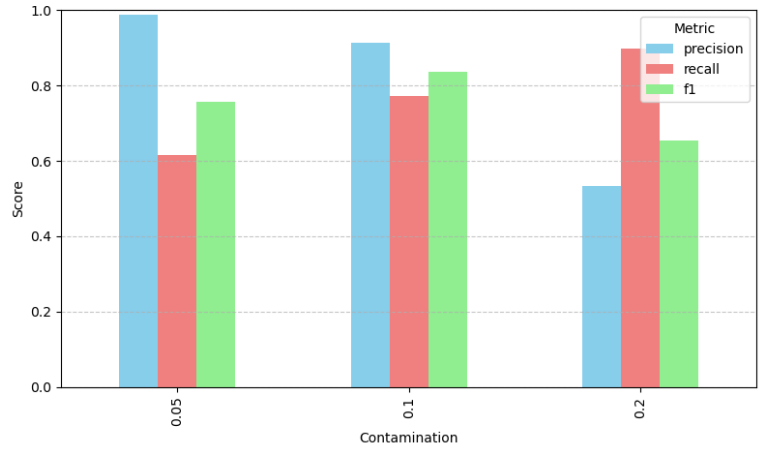


**Figure 15.** Effect of contamination ratio on Isolation Forest performance, with the number of trees equal to 500.

Additional experiments were also conducted using alternative machine learning algorithms, such as the One-Class Support Vector Machine (OC-SVM) (see Figure 16). Nevertheless, despite careful tuning of the kernel function and other hyperparameters, the OC-SVM consistently yielded lower performance compared with the Isolation Forest. Given these results, and considering the greater simplicity and industrial applicability of the proposed framework—which operates effectively without additional processing stages beyond feature extraction—the discussion in this work focuses primarily on the Isolation Forest outcomes.

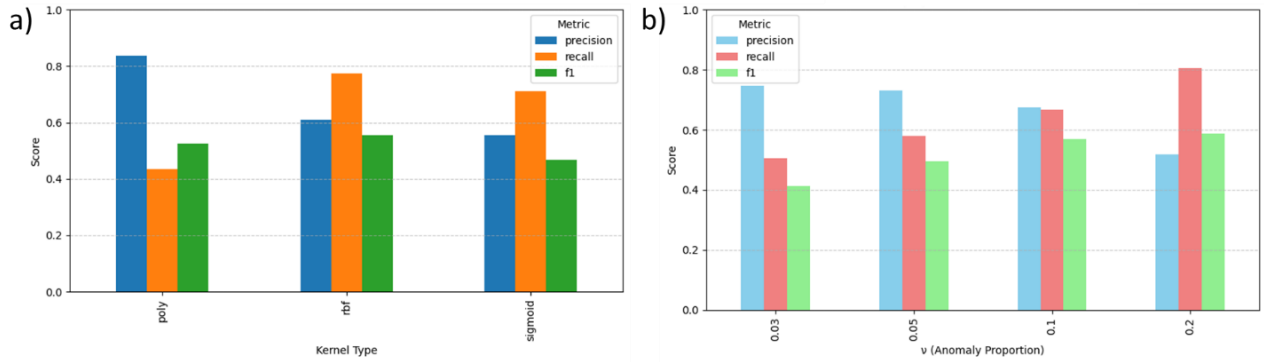


**Figure 16.** Results of OC-SVM algorithms when are varied the **(a)** kernel and **(b)** the $\nu$ hyeperarmeters.

*3.3. Scaling to a complex fabrication scenario*

As presented in Section 2, a component was printed and data collected. The process parameters employed for the production of this component differed from those used in the earlier experimental campaign, which was designed to assess the monitoring system's ability to interpolate between different frequency responses within the bounds of training but under new and unseen conditions. In particular, for this case the parameters were set as follows: −4 Ultim Arc, a welding speed of 732 mm/min, a wire feed speed of 2.8 m/min, and a welding voltage of 14.7 V. The deposition was generally stable, as confirmed by the images captured at the end of the process and by the analysis of the associated Isolation Forest based on time—frequency features (Figures 17 and 18, referring to the first and third layers, respectively).

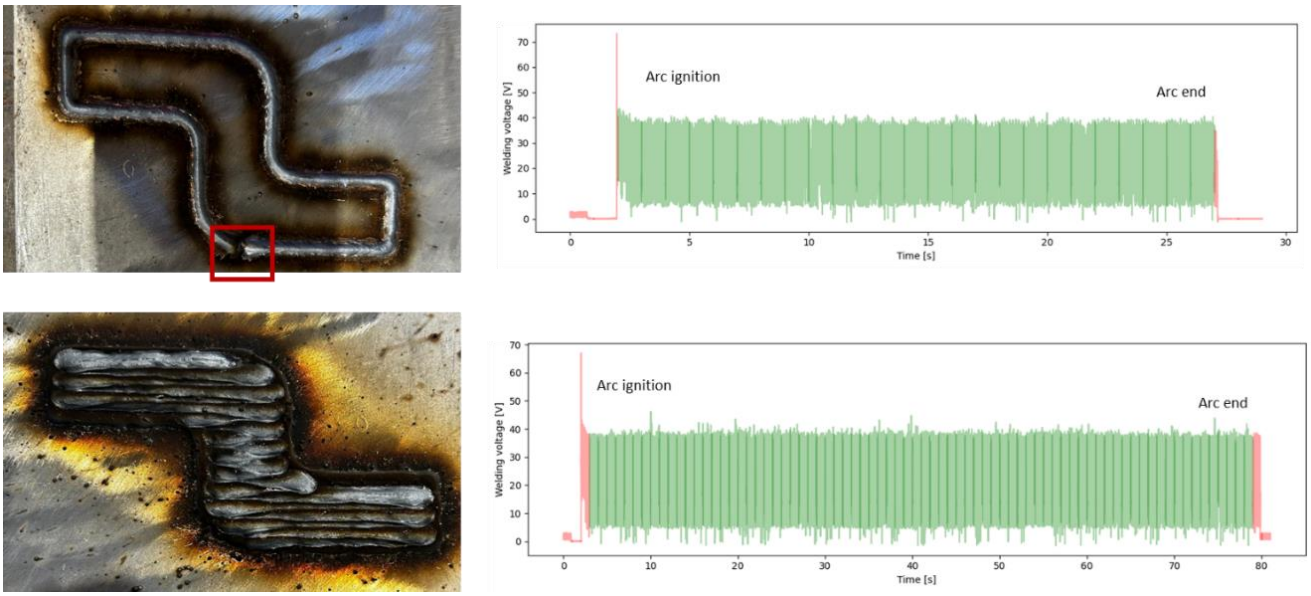


**Figure 17.** Results of the monitoring system at the end of the first layer.

As observed during the experiments, the main anomalies encountered were related to arc ignition failures or missing arc data. These cases were not included in the training of the Isolation Forest and were associated with some of the defects identified in the test dataset, where arc instability led to re-ignition events. When the arc was stable, the frequency content of the signals was consistent with defect-free deposition, and no anomalies were observed. However, during deposition, some defects did occur. These were primarily attributed to arc instability and inadequate heat dissipation. For example, in layer 7 (Figure 19), the torch

required cleaning for maintenance reasons. Due to the imperfect coverage caused by the unstable arc, the layer exhibited sub-optimal geometric filling that necessitated corrective cleaning. Although the alert system based on the Isolation Forest was not able to precisely localise the defect, it provided several warnings at the end of the deposition process. These warnings suggested the need for maintenance and inspection, which ultimately led to the discovery of a nozzle-related problem. In contrast, when control charts were employed, this anomalous condition was not detected. As illustrated in Figure 19d, no anomaly signal was generated, meaning that—without a dedicated anomaly detection module—no inspection would have been performed on this layer. This would likely have led to the perpetuation of the error, with the risk of developing more severe defects such as incomplete layer coverage, excessive porosity, or even full occlusions, which cannot be repaired.

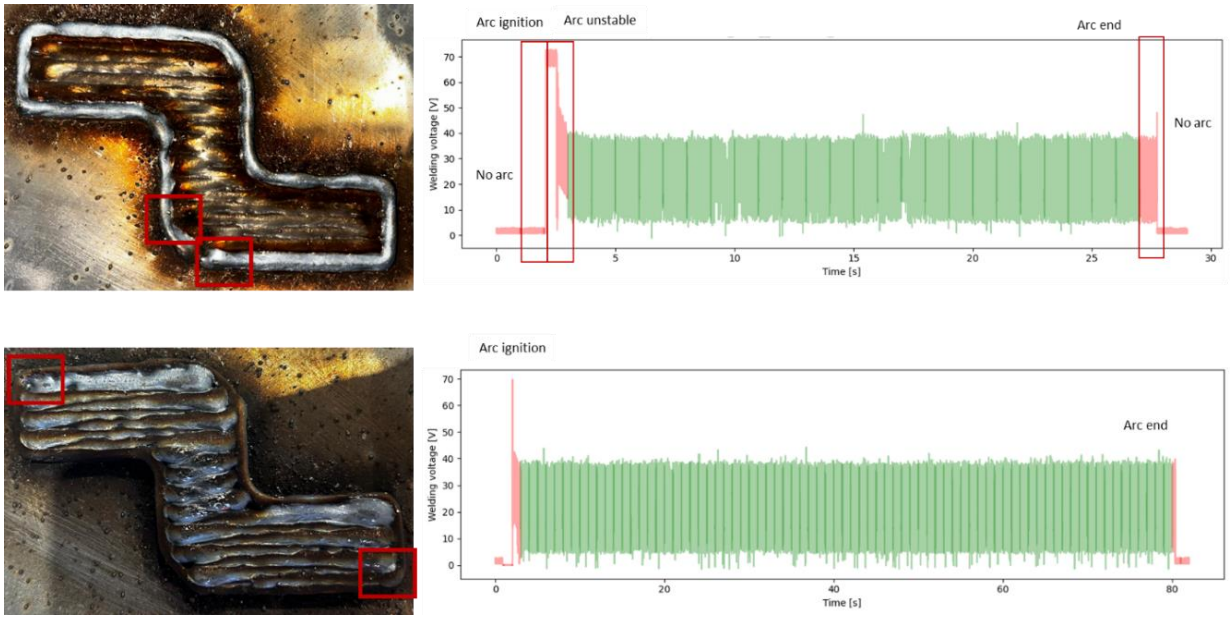


**Figure 18.** Results of the monitoring system at the end of the third layer.

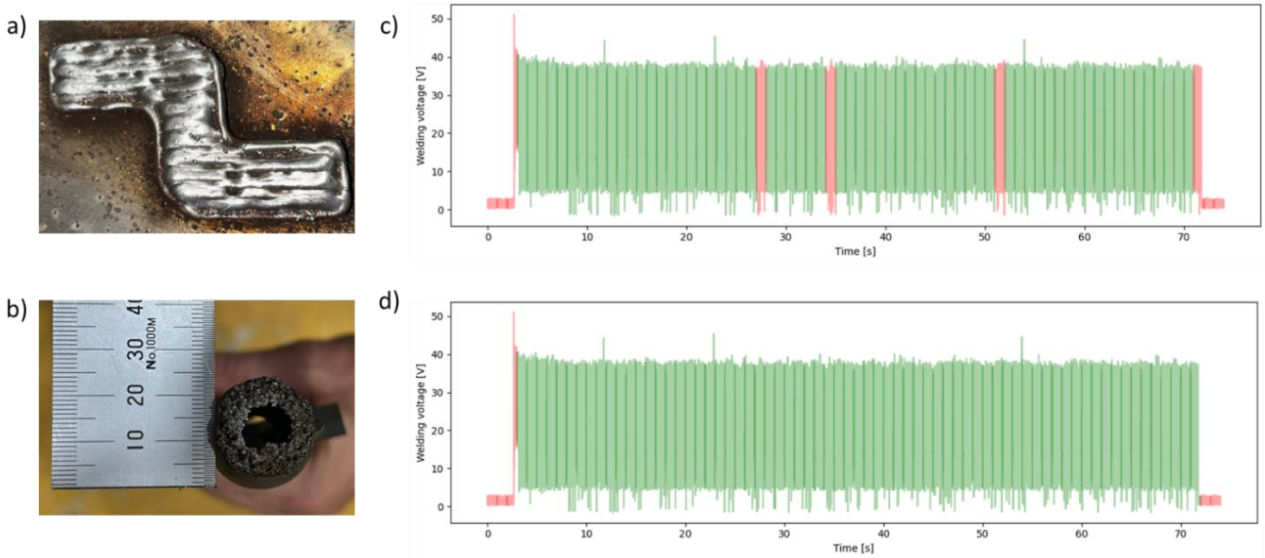


**Figure 19.** Results of the monitoring system on layer 7: **(a)** completed layer; **(b)** anomalous condition caused by nozzle contamination; **(c)** output of the Isolation Forest based on time–frequency features; and **(d)** output of the best-performing control chart applied to the welding voltage data.

### *3.4. Summary and final discussion*

In this work, we demonstrated and compared how process monitoring can be developed and implemented on a real system to assess the quality of printed parts. By collecting data during stable depositions, it is possible to learn the pattern of normal behaviour in the time–frequency domain and subsequently identify instabilities or anomalies that require warnings and equipment checks. The comparison between the proposed methodology and traditional control-chart-based approaches showed that, on the collected dataset, the F1-score was improved by 57%. Furthermore, when tested on a real component, conventional statistical process monitoring (SPM) methods were unable to detect anomalous conditions such as equipment wear. If left undetected and unresolved, such conditions can lead to the presence of defects in the part, including porosity, which critically undermines component integrity.

It is worth noting that the development of this methodology does not require class information or extensive data labelling. Instead, it can be applied in scenarios where only time-series data from defect-free depositions are available. This characteristic makes the approach particularly suitable as a guideline for data-limited cases. Although validated here for WA-DED, the methodology can be readily extended to conventional arc welding as well as other additive manufacturing processes. Moreover, its reliance solely on data from normal operations positions this approach within the scope of standardisation efforts. In fact, while traditional monitoring strategies based on control charts are typically linked to welding procedure specifications, the proposed methodology can achieve more effective results by exploiting the same or similar data sources.

### *3.5. Limitations and future works*

While the proposed methodology has demonstrated promising results, several limitations must be acknowledged. First, the localisation of anomalies within the deposited layers has not yet been achieved. The system can identify anomalous conditions and generate warnings but does not currently provide precise spatial mapping of defect locations, which would be essential for implementing targeted corrective actions during deposition. Second, the framework outputs anomalies in a qualitative form, without offering a consolidated quantitative measure of part quality. Future work will therefore focus on defining a quality index derived from anomaly detection outputs, enabling continuous and online tracking of deposition quality. Such an index would provide operators with a numerical metric to support decision-making and facilitate integration into quality assurance protocols. Moreover, the integration of the proposed approach into non-destructive testing (NDT) procedures represents a promising direction for future research, as it could further enhance process reliability and quality assessment. However, these developments would require substantially higher data flow and storage capacity, introducing a trade-off between monitoring performance and computational or infrastructural cost. Moreover, this work has primarily addressed wall-type depositions under stable process conditions. Other manufacturing scenarios require further investigation. For instance, in the case of overhanging structures, the absence of gravity-assisted support during deposition can cause distortions in the welding signals. Understanding how such distortions manifest and how they can be incorporated into anomaly detection models will be critical, especially given the potential of WA-DED to manufacture unsupported features. This capability is particularly attractive for the production of small-to-medium-sized components made of high-cost alloys such as titanium, Inconel, or Invar, where WA-DED offers advantages over powder-based AM

technologies. Future research will therefore concentrate on extending the methodology to these more complex geometries, improving defect localisation, and developing a quantitative quality index. Looking ahead, particular emphasis will be placed on generating realistic industrial impact through well-designed case studies and close collaboration with industry, ensuring that the approach evolves into a robust and standardisable tool for manufacturing practice.

## 4. Conclusion

In this work, we demonstrated and compared how process monitoring can be developed and implemented on a real WA-DED system to assess the quality of printed parts. The study was carried out using pulsed-GMAW with stainless steel 316L, supported by extensive data collection over 72 layers and validation on two printed walls that included both defect-free and defective regions. A methodology based on time–frequency feature extraction combined with an Isolation Forest model was proposed and benchmarked against traditional control-chart-based statistical process monitoring (SPM). The comparison showed that, on the collected dataset, the proposed approach improved the F1-score by 57% compared with control charts (from 54.3% to 85.3%). Both methodologies were further applied to a multi-bead, multi-layer component, where the proposed method again demonstrated promising performance in detecting process instabilities and enabling early maintenance checks, while SPM failed to identify certain conditions.

Nevertheless, some limitations remain. In particular, the current system does not localise defects within the layers, and the anomaly detection output remains qualitative rather than quantitative. Future research will therefore focus on: (i) extending the methodology to more complex scenarios such as overhanging structures, which are particularly relevant in WA-DED due to the absence of supports; (ii) improving defect localisation capability and detection performance; and (iii) developing a quantitative quality index to continuously track component integrity. Further investigations will also explore multi-sensor and multimodal data fusion, which could provide a more comprehensive basis for robust process monitoring in WA-DED and related additive manufacturing processes.

## Data availability statement

Data are available from the corresponding author upon reasonable request.

## Acknowledgments

This work was funded by INVITALIA with the project NEMESI. The authors would like to thank the Invitalia project NEMESI for supporting this research.

## Authors' contribution

Conceptualization, G.M., E.M., Z.P. and L.N.; methodology, G.M., E.M., Z.P. and L.N.; software, G.M. and E.M.; formal analysis, G.M., E.M., Z.P. and L.N; investigation, G.M, E.M., Z.P. and L.N.; resources, Z.P.; data curation, G.M, E.M.; writing—original draft preparation, G.M, E.M., Z.P. and L.N.; writing—review and editing, G.M, E.M., Z.P. and L.N.; visualization, G.M., E.M., Z.P. and L.N.; supervision, Z.P. and L.N.; project administration, Z.P. and L.N.; funding acquisition, Z.P. All authors have read and agreed to the published version of the manuscript.

## Conflicts of interests

The authors declare no conflict of interest.

## References


[1] Gao H, Li H, Shao D, Fang N, Miao Y, *et al.* Towards quality controllable strategies in wire-arc directed energy deposition. *Int. J. Extrem. Manuf.* 2025, 7(4):042004.

[2] Pattanayak S, Sahoo SK. Gas metal arc welding based additive manufacturing—a review. *CIRP J. Manuf. Sci. Technol.* 2021, 33:398–442.

[3] Sood A, Schimmel J, Ferreira VM, Bosman M, Goulas C, *et al.* Directed energy deposition of Invar 36 alloy using cold wire pulsed gas tungsten arc welding: effect of heat input on the microstructure and functional behaviour. *J. Mater. Res. Technol.* 2023, 25:6183–6197.

[4] Veiga F, Suárez A, Artaza T, Aldalur E. Effect of the heat input on wire-arc additive manufacturing of invar 36 alloy: microstructure and mechanical properties. *Weld. World* 2022, 66(6):1081–1091.

[5] Mattera G, Caggiano A, Nele L. Energy efficiency optimisation in wire arc additive manufacturing of invar 36 alloy via intelligent data-driven techniques. *Int. J. Precis. Eng. Manuf. Green Technol.* 2025, 12:905–917.

[6] Sideris I, Petrik J, Bambach M. Too hot to print, too slow to handle; finding optimal path characteristics for WAAM. *Manuf. Lett.* 2024, 41:879–890.

[7] Cui Q, Shao Z. A path planning and online compensation method for wire arc additive manufacturing of thin-walled curved hollow structure. *Int. J. Adv. Manuf. Technol.* 2025, 139:5855–5866.

[8] Norrish J, Cuiuri D. The controlled short circuit GMAW process: a tutorial. *J. Manuf. Processes* 2014, 16(1):86–92.

[9] Chen D, Chen H, Zhang G, Xiong J. Towards automatic control of process stability for thick-wall parts in arc-directed energy deposition based on arc voltage sensing. *J. Manuf. Processes* 2025, 141:250–262.

[10] Wu B, Pan Z, Ding D, Cuiuri D, Li H, *et al.* A review of the wire arc additive manufacturing of metals: properties, defects and quality improvement. *J. Manuf. Processes* 2018, 35:127–139.

[11] Shin SJ, Hong SH, Jadhav S, Kim DB. Detecting balling defects using multisource transfer learning in wire arc additive manufacturing. *J. Comput. Des. Eng.* 2023 10(4):1423–1442.

[12] Mattera G, Nele L, Paolella D. Monitoring and control the wire arc additive manufacturing process using artificial intelligence techniques: a review. *J. Intell. Manuf.* 2024, 35(2):467–497.

[13] Li R, Ma H, Wang R, Song H, Zhou X, *et al.* Application of unsupervised learning methods based on video data for real-time anomaly detection in wire arc additive manufacturing. *J. Manuf. Processes* 2025, 143:37–55.

[14] Xiong J, Zhang Y, Pi Y. Control of deposition height in WAAM using visual inspection of previous and current layers. *J. Intell. Manuf.* 2021, 32(8):2209–2217.

[15] Wang Y, Xu X, Zhao Z, Deng W, Han J, *et al.* Coordinated monitoring and control method of deposited layer width and reinforcement in WAAM process. *J. Manuf. Processes* 2021, 71:306–316.

[16] Mu H, He F, Yuan L, Commins P, Xu J, *et al.* High-frequency real-time bead geometry measurement in wire arc additive manufacturing based on welding signals. *IEEE Trans. Ind. Inf.* 2025, 21(3):2630–2639.

[17] Chabot A, Rauch M, Hascoët JY. Novel control model of Contact-Tip-to-Work Distance (CTWD) for sound monitoring of arc-based DED processes based on spectral analysis. *Int. J. Adv. Manuf. Technol.* 2021, 116(11–12):3463–3472.

[18] Franke J, Heinrich F, Reisch RT. Vision based process monitoring in wire arc additive manufacturing (WAAM). *J. Intell. Manuf.* 2025, 36(3):1711–1721.

[19] Li R, Ma H, Cong B, Shi Y, Zeng C, *et al.* Lightweight You Only Look Once-based automatic defect detection in wire arc additive manufacturing. *Mater. Sci. Addit. Manuf.* 2025, 4(4):025210035.

[20] Li Y, Polden J, Pan Z, Cui J, Xia C, *et al.* A defect detection system for wire arc additive manufacturing using incremental learning. *J. Ind. Inf. Integr.* 2022, 27:100291.

[21] Mattera G, Nel L. Machine learning approaches for real-time process anomaly detection in wire arc additive manufacturing. *Int. J. Adv. Manuf. Technol.* 2025, 137:2863–2888.

[22] Surovi NA, Soh GS. Acoustic feature based geometric defect identification in wire arc additive manufacturing. *Virtual Phys. Prototyp.* 2023, 18(1):e2210553.

[23] Xiong J, Zhang G. Online measurement of bead geometry in GMAW-based additive manufacturing using passive vision. *Meas. Sci. Technol.* 2013, 24(11):115103.

[24] Dong K, Wu Q, Qin X, Hu Z, Hua L. In-situ optical monitoring and analysis of weld pool based on machine vision for wire and arc additive manufacturing. *Int. J. Adv. Manuf. Technol.* 2024, 133(9–10):4865–4878.

[25] Nguyen VA, Supriadi D, Xuan NH, Van Tuan N, Le VT, *et al.* Melt pool dynamics and droplet transfer in single-layer wire and arc additive manufacturing process. *Prog. Addit. Manuf.* 2025, 10(10):8127–8138.

[26] Zhou X, Zheng S, Li R, Xiong X, Yuan Y, *et al.* Improved YOLOv5-based pore defect detection algorithm for wire arc additive manufacturing. *Mater. Today Commun.* 2024, 39:108710.

[27] Mattera G, Polden J, Norrish J. Monitoring the gas metal arc additive manufacturing process using unsupervised machine learning. *Weld. World* 2024, 68:2853–2867.

[28] Cook GE, Maxwell JE, Barnett RJ, Strauss AM. Statistical process control application to weld process. *IEEE Trans. Ind. Appl.* 1997, 33(2):454–463.

[29] Thekkuden DT, Santhakumari A, Sumesh A, Mourad AHI, Rameshkumar Kjtij. Instant detection of porosity in gas metal arc welding by using probability density distribution and control chart. *Int. J. Adv. Manuf. Technol.* 2018, 95:4583–4606.

[30] Shin S, Jin C, Yu J, Rhee S. Real-time detection of weld defects for automated welding process base on deep neural network. *Metals (Basel)* 2020, 10(3):389.

[31] Vasan V, Sridharan NV, Balasundaram RJ, Vaithiyanathan S. Ensemble-based deep learning model for welding defect detection and classification. *Eng. Appl. Artif. Intell.* 2024, 136:108961.

[32] Sumesh A, Nair BB, Rameshkumar K, Santhakumari A, Raja A, *et al.* Decision tree based weld defect classification using current and voltage signatures in GMAW process. *Mater. Today Proc.* 2018, 5(2):8354–8363.

[33] Chandola V, Banerjee A, Kumar V. Anomaly detection. *ACM Comput. Surv.* 2009, 41(3):1–58.

[34] Omar S, Ngadi A, Jebur HH. Machine learning techniques for anomaly detection: an overview. *Int. J. Comput. Appl.* 2013, 79(2):33–41.

[35] Mattera G, Vozza M, Polden J, Nele L, Pan Z. Frequency informed convolutional autoencoder for *in situ* anomaly detection in wire arc additive manufacturing. *J. Intell. Manuf.* 2024, 36:5819–5834.

[36] Montgomery DC. The 100th anniversary of the control chart. *J. Qual. Technol.* 2024, 56(1):2–4.

[37] He QP, Wang J. Statistical process monitoring as a big data analytics tool for smart manufacturing. *J. Process Control* 2018, 67:35–43.

[38] Mattera G, Yap EW, Polden J, Brown E, Nele L, *et al.* Utilising unsupervised machine learning and IoT for cost-effective anomaly detection in multi-layer wire arc additive manufacturing. *Int. J. Adv. Manuf. Technol.* 2024, 135:2957–2974.

[39] Liu FT, Ting KM, Zhou ZH. Isolation forest. In *8th IEEE International Conference on Data Mining (ICDM 2008)*, Pisa, Italy, December 15–19, 2008, pp. 413–422.